Structural analysis of the antimalarial drug halofantrine by means of Raman spectroscopy and density functional theory calculations

Torsten Frosch
Jürgen Popp
Friedrich-Schiller-Universität Jena
Institut für Physikalische Chemie
Helmholtzweg 4
Jena, D-07743 Germany
and
Institut für Photonische Technologien
Albert-Einstein-Straße 9
Jena, D-07745 Germany

Abstract. The structure of the antimalarial drug halofantrine is analyzed by means of density functional theory (DFT) calculations, IR, and Raman spectroscopy. Strong, selective enhancements of the Raman bands of halofantrine at 1621 and 1590 cm^{-1} are discovered by means of UV resonance Raman spectroscopy with excitation wavelength $\lambda_{exc}=244$ nm. These signal enhancements can be exploited for a localization of small concentrations of halofantrine in a biological environment. The Raman spectrum of halofantrine is calculated by means of DFT calculations [B3LYP/6-311+$G(d,p)$]. The calculation is very useful for a thorough mode assignment of the Raman bands of halofantrine. The strong bands at 1621 and 1590 cm^{-1} in the UV Raman spectrum are assigned to combined C=C stretching vibrations in the phenanthrene ring of halofantrine. These bands are considered as putative marker bands for $\pi\pi$ interactions with the biological target molecules. The calculation of the electron density demonstrates a strong distribution across the phenanthrene ring of halofantrine, besides the electron withdrawing effect of the Cl and CF_3 substituents. This strong and even electron density distribution supports the hypothesis of $\pi\pi$ stacking as a possible mode of action of halofantrine. Complementary IR spectroscopy is performed for an investigation of vibrations of polar functional groups of the halofantrine molecule.
[DOI: 10.1117/1.3432656]

Keywords: halofantrine; malaria; drug design; Raman spectroscopy; ultraviolet resonance Raman; density functional theory; electron density distribution.

Paper 09439SSR received Oct. 1, 2009; revised manuscript received Oct. 29, 2009; accepted for publication Nov. 5, 2009; published online Jul. 7, 2010.

1 Introduction

Malaria is a major human parasitic disease and affects approximately 40% of the world population.[1–3] The mortality and morbidity from the disease strongly increased in the recent decades. The disease has tremendous effects on the economic development primarily of sub-Saharan countries.[1,2] The control of malaria was declared as a global priority by the World Health Organization[2] (WHO). The main reason for this disaster is a rise of worldwide resistances against existing drugs, most of all against chloroquine.[1–4] Chloroquine was the mainstay therapy for decades and is one of the most important drugs used against an infectious disease.[5,6] To address these problems with resistances, more effort is required in the development of novel antimalarials.[3,4] In particular, a better understanding of the molecular mode of action of the active agents is required for the design of structure-based drugs.

Halofantrine is a drug that is effective against chloroquine-resistant strains of *Plasmodium falciparum*[7] and *Plasmodium vivax*.[8] Halofantrine was first synthesized by Colwell et al.[9] in an army research program on malaria, within a large series of phenanthrenes, quinolines, and related arylaminoethanols. The drug is marketed by GlaxoSmithKline under the name Halfan. Halofantrine was also successfully applied in a pediatric study.[10] The drug shows enhanced activity in combination with chloroquine[11] and is especially prescribed against a high incidence of multidrug resistances.[12]

However, the molecular mode of action of halofantrine is not well understood. The drug interferes with the detoxification process of hemoglobin digestion by-products in the 48-h cycle of the red blood cell state of the malaria parasite *Plasmodium*.[13–18] It was shown that protein mutations in *P. falciparum* confer resistances to halofantrine.[19] Recently a crystal structure of a complex of halofantrine and ferriprotoporphyrin IX (FPPIX) was derived and it was found that $\pi\pi$ stacking of the phenanthrene ring of the drug and the porphyrin of the target structure may play a major role in the biological activity.[20,21] Halofantrine inhibits the formation of the malaria pigment hemozoin. Therefore, a selective binding to

Address all correspondence to: Torsten Frosch, Friedrich-Schiller-Universität Jena, Institut für Physikalische Chemie, Helmholtzweg 4, Jena, D-07743 Germany. Tel: 49-3641-206221; E-mail: torsten.frosch@uni-jena.de

1083-3668/2010/15(4)/041516/9/$25.00 © 2010 SPIE

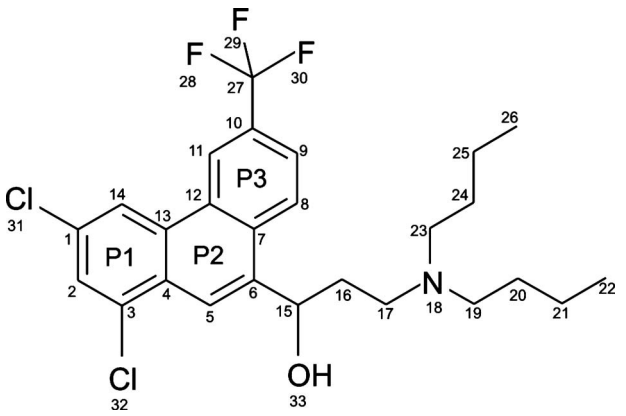

Fig. 1 Molecular structure of halofantrine. The atomic numbering scheme and the partitioning of the phenanthrene ring in P1, P2, and P3 is used in the context for the description of the mode assignment.

the small, active growing faces of the hemozoin crystallites may be considered as a mode of action.[22,23] Halofantrine showed essential chemical features in a pharmacophore model for FPPIX-targeting antimalarials.[24]

New diagnostic techniques are required to elucidate the molecular mode of action of halofantrine *in vitro* as well as in *Plasmodium*. Therefore, the fast, easy, and reliable localization of the drug in the biological environment is of high importance. Halofantrine was determined in rat[25] and human[12,26] plasma by means of high-performance liquid chromatography (HPLC). However, a localization of halofantrine in life cells with high spatial resolution would be desired to address the specific binding sides of the drugs in *Plasmodium*. Novel photonic diagnostic techniques were recently developed and exciting results were achieved in biomedical research.[27–37] The application of such biophotonic techniques has high potential to elucidate the molecular mode of action of halofantrine and to contribute in a structure-based design of new, effective drugs against malaria.

2 Material and Methods

2.1 *Chemicals*

Halofantrine hydrochloride was a kind gift of GlaxoSmith-Kline and was used without further purification. The systematic IUPAC name of halofantrine is 3-dibutylamino-1-[1,3-dichloro-6-(trifluoromethyl) phenanthren-9-yl]-propan-1-ol. The molecular structure of halofantrine is shown in Fig. 1. The atomic numbering scheme and the partitioning of the phenanthrene ring in P1, P2 and P3 in Figure 1 is used in the context for the description of the mode assignment.

2.2 *Spectroscopy*

The Fourier transform (FT) Raman spectrum of halofantrine hydrochloride was recorded with a Bruker FT Raman spectrometer (RFS 100/S) at the macroscopic mode with a spectral resolution of 2 cm^{-1}. The instrument was equipped with a Nd:YAG laser ($\lambda_{exc}=1064$ nm, estimated laser power at the samples $P=50$ mW) as the excitation source and a liquid-nitrogen-cooled germanium detector.

The complementary FT IR spectrum of halofantrine hydrochloride was measured as KBr pellet using a Bruker IFS 66 spectrometer equipped with a DTGS (doped triglycerinsulfate) detector and with 4-cm^{-1} spectral resolution.

UV resonance Raman microspectroscopy was performed with an UV Raman setup (HR800 LabRam, Horiba/Jobin-Yvon, focal length of 800 mm and a 2400 lines/mm grating) equipped with an Olympus BX41 microscope, UV sensitive video camera, and a liquid-N_2-cooled CCD detector. For UV microscopy, a UV achromatic fused silica/CaF_2 microspot objective [LMU-40×-UVB, numerical aperture (NA)=0.5] with broad band UVB coating was chosen. Validation of the wave number axis was performed via the Raman signals from Teflon. The excitation wavelength 244 nm was derived from an intracavity frequency-doubled argon-ion laser (Innova300-MotoFreD, Coherent Inc.). The laser power at the sample was estimated to be 1 mW. The spectral resolution was 5 cm^{-1}. Because the laser wavelength was chosen to excite the sample in an electronic absorption band, it was necessary to carefully avoid any sample destruction. Furthermore, the sample rotation technique[37,38] was applied.

2.3 *Density Functional Theory Calculation*

Density functional theory (DFT) calculations were performed with Gaussian 03 (revision D.01)[39] with Becke's three-parameter exchange functional[40] (B3) as slightly modified by Stephens et al.,[41] coupled with the correlation functional of Lee et al.[42] (B3LYP) and B3 in combination with the correlation part of the functional from Perdew and Wang[43] and Perdew et al.[44] (B3PW91). Double $(6\text{-}31+G(d,p))$ and triple $(6\text{-}311+G(d,p))$ split valence basis sets of contracted Gaussian functions with polarized and diffuse functions[45–47] were applied. These hybrid exchange correlation functionals provide reliable estimates of experimental frequencies of organic molecules with small root mean square deviations.[48–53]

The DFT calculated harmonic vibrational frequencies are typically too large compared with the experimentally observed ones, due to neglect of anharmonicity, incomplete incorporation of electron correlation, and the use of finite basis sets. Fortunately, this overestimation of the calculated harmonic vibrational frequencies is relatively uniform and can be circumvented by applying transferable scaling factors to the harmonic frequencies.[48,54] For the B3LYP/$6\text{-}311+G(d,p)$ calculations, values of 0.98 for modes below 1800 cm^{-1} and 0.96 above 1800 cm^{-1} were applied, in agreement with the literature.[54–60]

The calculated Raman activities were transformed into Raman intensities[61] and were further convoluted with Gauss-Lorentz-weighted profiles to simulate Raman spectra with finite bandwidth.

3 Results and Discussion

Raman spectroscopy has unique capabilities as diagnostic tool in biomedical research.[27–37] The method is highly specific for slight environmental changes that have importance in the biological activity of molecules—such as changes in pH,[55] water environment,[56] or molecular interactions.[35,37] The measurement is fast and does not require further labeling or preparation steps. The combination of a Raman spectrometer with a confocal microscope enables targeting of biological molecules in subcellular compartments with a spatial resolution of ap-

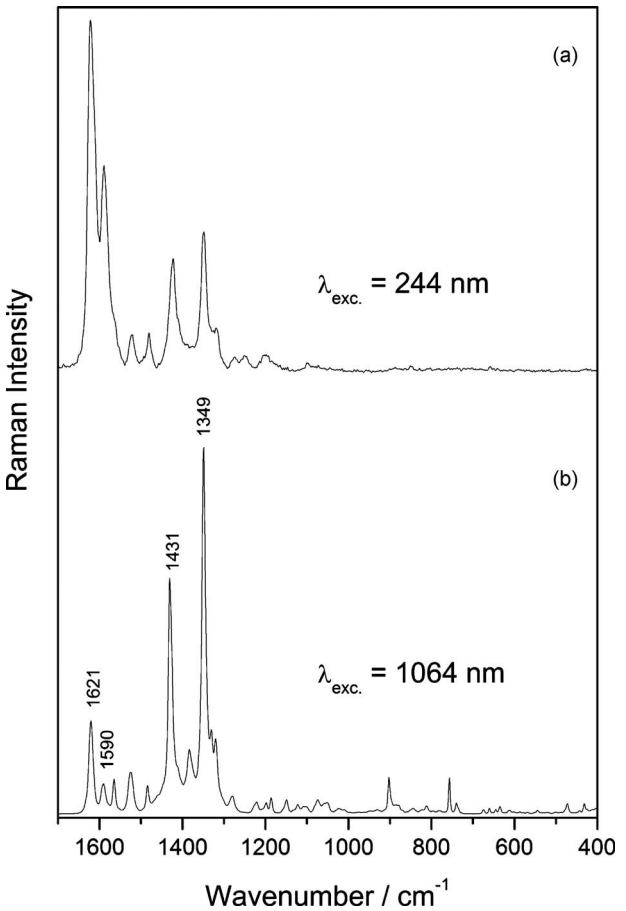

Fig. 2 (a) UV resonance Raman spectrum of halofantrine (λ_{exc}=244 nm) and (b) FT-Raman spectrum of halofantrine (λ_{exc} =1064 nm). The wavenumber values of some prominent bands are given in graph (b). The band at 1621 cm^{-1} is very strong in the UV Raman spectrum (a) due to the resonance enhancement. The intensities in both graphs are normalized to the strongest peak in the spectra, respectively.

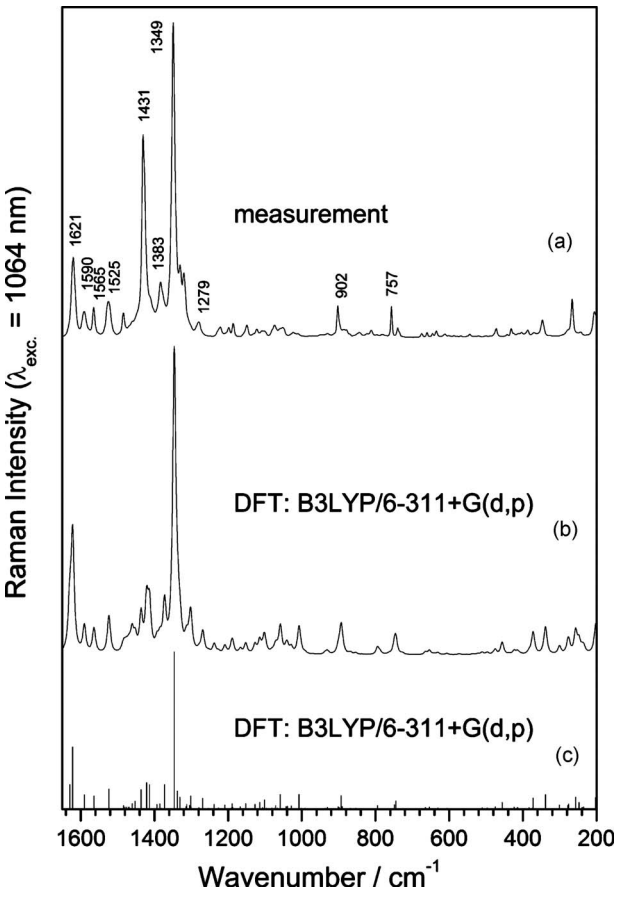

Fig. 3 Comparison of an experimental FT Raman spectrum (λ_{exc} =1064 nm) of halofantrine (a) alongside a calculated [B3LYP/6-311 + $G(d,p)$] Raman profile (b). The individual Raman modes of the convoluted profile (b) are shown in the stick spectrum (c). The wave number values of some prominent bands are given in (a).

prox. 0.5 μm.[33,62] Living cells can be studied since water is a weak Raman scatterer and the technique is nondestructive. The sensitivity and selectivity of Raman spectroscopy can be further improved if the excitation wavelength is tuned into the electronic absorption of the molecules.[30,33,63–65] Resonance Raman spectroscopy is an extremely capable technique and enables a selective enhancement of the Raman signals of chromophores in complex biological environments.[33,63]

Furthermore, the application of UV laser excitation wavelengths causes very strong signal enhancements due to the intrinsic enhancement of the scattering effect [$I(\omega) \sim \omega^4$] and the resonance enhancement of vibrations that are coupled to the electronic transitions.[55,56,58] Additionally, the Raman signals are spectrally shifted with respect to disturbing fluorescence and it is possible to derive Raman spectra with high contrast within an environment with fluorescing background.[58,66] UV resonance Raman microspectroscopy was applied for a localization of small amounts of antimalarial drugs in plant material.[56,58]

3.1 *UV Resonance Raman Spectroscopy*

The molecular structure of halofantrine (Fig. 1) shows a chromophoric phenanthrene structure that is highly polarizable and causes strong Raman signals [Fig. 2(b)]. These Raman intensities can be enhanced by several magnitudes by exploitation of the described UV resonance effect. Halofantrine shows strong absorption bands in the deep UV at approx. 250 nm.[67] Therefore, the laser excitation wavelengths λ_{exc} =244 nm was chosen for the investigation of halofantrine. A strong enhancement of two Raman bands at 1621 and 1590 cm^{-1} is seen in the UV resonance Raman spectrum [Fig. 2(a)] in comparison with the nonresonant FT Raman spectrum (λ_{exc}=1064 nm) [Fig. 2(b)]. These strongly enhanced Raman signals of halofantrine can be used as marker bands to localize halofantrine in a complex biological environment. The intensities in the spectra in Fig. 2 are normalized to the strongest Raman peaks, respectively, for better illustration.

3.2 *DFT Calculation*

3.2.1 *Raman spectra*

To interpret the individual Raman bands in more detail, a thorough normal mode assignment is required. High-performance computing facilities nowadays enable a reliable

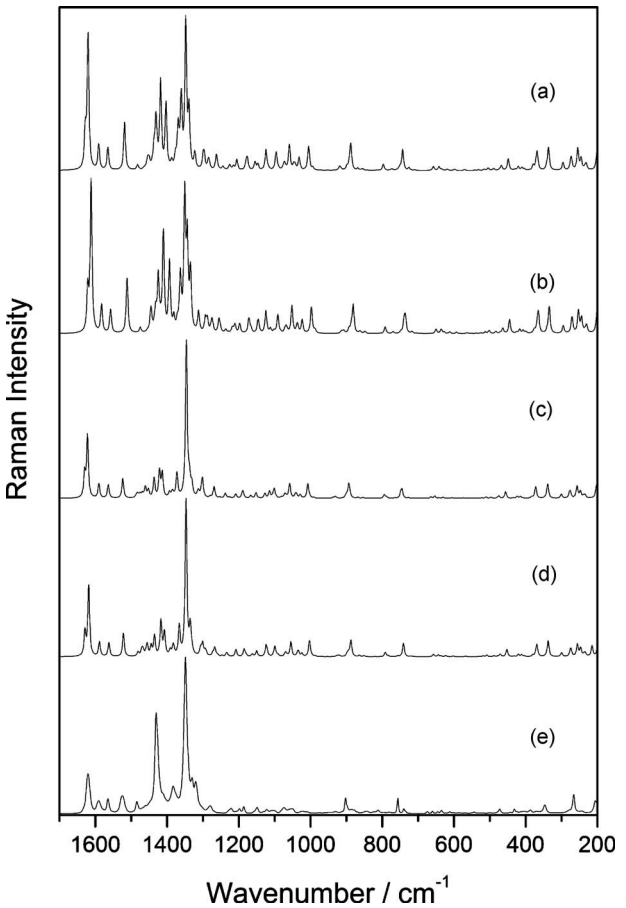

Fig. 4 Comparison of measured (e) and calculated Raman spectra (a–d) of halofantrine with different model chemistries. The convolution of the profiles was performed with FWHM 6 instead of FWHM 10 in Fig. 3(b). (a) DFT calculation of the Raman spectrum of halofantrine [B3PW91/6-311+$G(d,p)$], (b) DFT calculation of the Raman spectrum of halofantrine [B3PW91/6-31+$G(d,p)$], (c) DFT calculation of the Raman spectrum of halofantrine [B3LYP/6-311+$G(d,p)$], (d) DFT calculation of the Raman spectrum of halofantrine [B3LYP/6-31+$G(d,p)$], (e) Measured FT Raman spectrum of halofantrine (λ_{exc}=1064 nm).

calculation of vibrational spectra of medium-sized biomolecules.[33,58] The DFT calculation [B3LYP/6-311+$G(d,p)$] of the Raman spectrum of halofantrine is shown in Fig. 3. The individual Raman bands in the calculated stick spectrum [Fig. 3(c)] were convoluted with line profiles [Fig. 3(b)] for comparison with measured Raman spectra with finite bandwidth [Fig. 3(a)]. One can see that often several normal modes contribute to an individual Raman band. However, the strongest peak in the nonresonant Raman spectrum of halofantrine [Fig. 3(b)] is dominated by one distinct mode at 1347 cm^{-1} [Fig. 3(c)]. Several weaker normal modes contribute to the wings of the line profile of this band. Two molecular vibrations at 1621 cm^{-1} and weaker at 1629 cm^{-1} [Fig. 3(c)] contribute to the Raman peak at 1621 cm^{-1} [Fig. 3(b)], which is strongly enhanced in the UV resonance Raman spectrum of halofantrine [Fig. 2(a)]. The overall agreement of the calculated Raman spectrum of halofantrine [Fig. 3(b)] and the measurement [Fig. 3(a)] is very good, while the intensity of the band at 1431 cm^{-1} is underestimated in the calculation. DFT calculations with the hybrid functional B3PW91 were performed to address whether any improvement can be achieved (results are shown in Fig. 4). The calculation with B3PW91 shows an improvement of the intensity of the Raman band at 1431 cm^{-1}; however, the intensity of the band at 1621 cm^{-1} is overestimated. The results of the DFT calculations with double [6-31+$G(d,p)$] [Figs. 4(b) and 4(d)] and triple [6-311+$G(d,p)$] [Figs. 4(a) and 4(c)] split valence basis sets are very similar and no significant basis size effect was found. The calculation with the model chemistry B3LYP/6-311+$G(d,p)$ was chosen for further consideration because of the very good agreement in the wavenumber region 1500 to 1650 cm^{-1}, where certain Raman modes gain strong UV resonance enhancement.

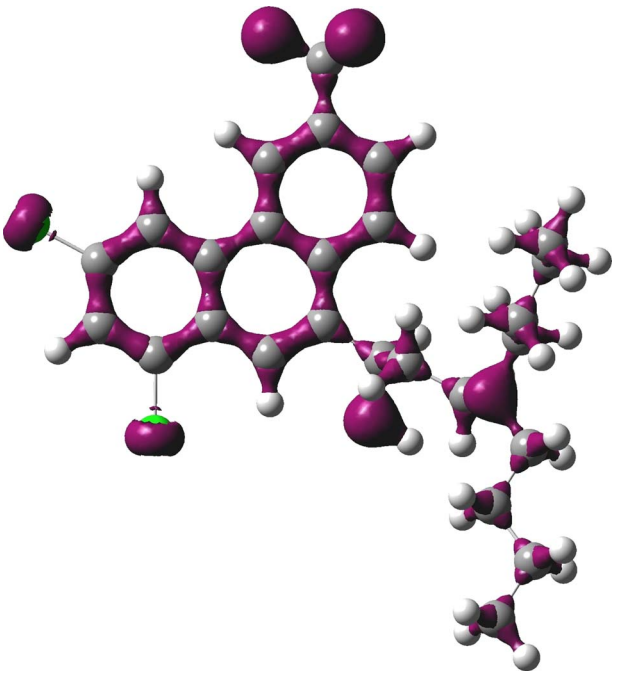

Fig. 5 Calculation of the electron density distribution of halofantrine (iso-value 0.25 electrons/a_0^3). An even electron distribution is seen in the phenanthrene ring of halofantrine, despite the electron withdrawing effect of substituents C(1)Cl(31) and C(3)Cl(32) as well as C(27)F(28)F(29)F(30).

3.2.2 *Electron density distribution*

The electron density distribution of halofantrine was calculated and yields fundamental insight regarding the possible binding behavior of the halofantrine molecule. A $\pi\pi$ stacking of the phenanthrene ring of halofantrine with the porphyrin backbone of ferriprotoporphyrin IX (FPPIX) was found[20,21] in a recent crystal structure of an *in vitro* complex of halofantrine with FPPIX. One should consider whether such binding is possible, due to strongly electron withdrawing substituent's at the phenanthrene ring of halofantrine. The electron density distribution of halofantrine (Fig. 5) highlights the electron withdrawing effect of the substituent's [C(1)Cl(31) and C(3)Cl(32) as well as C(27)F(28)F(29)F(30)]. However, a strong and evenly distributed electron density remains across the phenanthrene ring. This result supports the hypothesis that

$\pi\pi$ stacking may play an important role in the biological activity of halofantrine.

3.3 *Mode Assignment and Atomic Displacements*

The ultimate goal of the Raman spectroscopic investigation of halofantrine is a localization of the drug at the binding side of the biological target in life cells and an elucidation of changes in the Raman spectrum, caused by molecular interactions. To enable a discussion of such changes in the Raman bands of halofantrine, caused by changes in the environment, a detailed interpretation of the individual Raman bands is required. The DFT calculations can be used for a thorough band assignment. The calculations of the atomic displacements of the molecular normal modes provide much deeper understanding of the associated Raman bands.

The Raman spectrum of halofantrine consists of two well separated parts above 2800 cm^{-1} and below 1800 cm^{-1} (see Fig. 6). The range with high wave number values consist of two separated parts: a region with CH-stretching vibrations at the phenanthrene ring (3120 to 3060 cm^{-1}) and an area with CH_2, CH_3 stretching vibrations at the side chain (3010 to 2840 cm^{-1}) of halofantrine. In addition, there is also one OH stretching vibration present at 3710 cm^{-1}. However, the fingerprint region of halofantrine (below 1800 cm^{-1}) is of more importance in the further discussion. The graphical illustration of the atomic displacements of two prominent modes at 1621 and 1349 cm^{-1} are shown in Figs. 7(a) and 7(b), respectively. The assignment of more Raman bands of halofantrine is summarized in Table 1.

The strongest peak in the UV resonance Raman spectrum (λ_{exc}=244 nm) of halofantrine (Fig. 1) is found at wavenumber position 1621 cm^{-1} [Fig. 2(a)]. This band is assigned to a very strong, combined C═C-stretching vibration at the phenanthrene ring. The atomic displacement of the mode is displayed in Fig. 7(a). The strongest contribution to this normal mode arises from νC(5)═C(6) in P2 (see Fig. 1 for numbering scheme) as well as from νC(6)—C(15) at the connection of the side chain of the molecule and δ_{ip}C(5)H. A highly symmetric vibration is seen across the phenanthrene ring, where νC(1)═C(14), νC(3)═C(4), νC(13)═C(12), νC(5)═C(6), νC(11)═C(10), and νC(7)═C(8) stretch in phase, with a parallel, out-of-phase movement of the pairs {C(4), C(7)} and {C(12), C(9)} toward each other, respectively. Further bending contributions take place δ_{ip}C(14)H, δ_{ip}C(11)H and weaker δ_{ip}C(9)H and δ_{ip}C(8)H. The fluorine atoms F(28), F(29), and F(30) and chlorine atoms Cl(31) and Cl(32) are fixed in space. There are no contributions from the side chain. The very strong enhancement of this mode in the UV resonance Raman spectrum [Fig. 2(a)] is very promising, since this combined C═C-stretching vibration is likely to be influenced by $\pi\pi$ stacking of the phenanthrene ring to the porphyrin ring of biological target structures.[20,21] The calculation of the electron density distribution of halofantrine supports the hypothesis of such interaction. The monitoring of changes in this Raman band during the drug-target interaction might yield novel insight into proposed biological activities of halofantrine.

The strongest band in the nonresonant Raman spectrum is seen at wavenumber position 1349 cm^{-1} [Fig. 2(b)]. Two different snapshots of the atomic displacement of this mode are illustrated in Fig. 7(b). The normal mode consists of a very strong, combined CC-stretching vibration at the phenanthrene ring, an in-phase breathing vibration at [C(4)C(13), C(7)C(12)] of P1, P2, and P3; combined with a deformation mode [see Fig. 7(b)]. The symmetric narrowing of the ring system at C(4)C(13) and C(7)C(12) is nicely illustrated in the two snapshots of the molecular vibration in Fig. 7(b). More contributions to this mode arise from νC(10)C(27) and νC(27)F_3 as well as very strong δ_{ip}C(9)H, δ_{ip}C(8)H, δ_{ip}C(11)H, and δ_{ip}C(14)H and medium δ_{ip}C(2)H, δ_{ip}C(5)H, and δ_{ip}C(15)H vibrations. Small ωCH_2 contributions are present at the side chain.

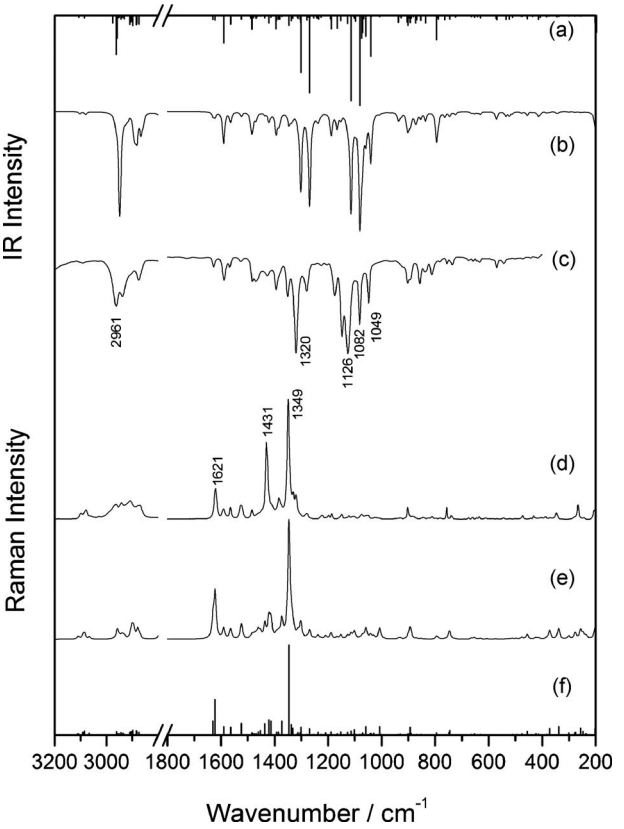

Fig. 6 Comparison of measured and calculated [B3LYP/6-311 + $G(d,p)$] vibrational spectra of halofantrine. Two scaling factors were applied: 0.98 for wave numbers smaller than 1800 cm^{-1} and 0.96 for those above. (a) DFT calculation of the IR stick spectrum of halofantrine, (b) DFT calculation and convolution of the IR spectrum of halofantrine, (c) measured FT IR spectrum of halofantrine, (d) measured FT Raman spectrum of halofantrine, (e) DFT calculation and convolution of the Raman spectrum of halofantrine, and (f) DFT calculation of the Raman stick spectrum of halofantrine. The IR and Raman spectra of halofantrine are complementary. Distinct normal modes show either strong IR or Raman activity, respectively. The wavenumber values of some prominent IR/Raman bands are given in (c) and (d), respectively.

3.4 *IR Spectroscopy*

The IR and Raman spectra of halofantrine yield complementary information. Highly symmetric C═C-stretching vibrations in the phenanthrene ring [e.g., Figs. 7(a) and 7(b)] posses strong changes in polarizability and cause intense bands in the Raman spectrum (Figs. 2 and 3). On the other hand, polar

Table 1 Mode assignment and wave number values of prominent Raman bands of halofantrine [Figs. 2, 3, and 6].

$\tilde{\nu}$(cm^{-1})	Assignment
3120–3060	Localized νCH at phenanthrene ring
3010–2840	νCH_2, νCH_3 at side chain
1621	Very strong C═C stretching vibration at the phenanthrene ring; strongest contribution by νC(5)═C(6) in P2 as well as C(6)—C(15) at the connection of the side chain and δ_{ip}C(5)H; highly symmetric vibration across the phenanthrene ring: νC(1)—C(14), νC(3)—C(4), νC(13)—C(12), νC(5)—C(6), νC(11)—C(10), and νC(7)—C(8) stretch in phase, with a parallel, out-of-phase movement of the atom pairs {C(4), C(7)} and {C(12)C(9)} toward each other, respectively; further bending: δ_{ip}C(14)H, δ_{ip}C(11)H and weaker δ_{ip}C(9)H and δ_{ip}C(8)H; F(28), F(29), F(30), Cl(31), and Cl(32) are fixed in space; no contribution from the side chain
1590	Strong C═C stretching vibration at the phenanthrene ring; dominated by in-phase C(2)═C(3) and C(14)═C(13) stretching in P1, C(1)═C(14) and C(3)═C(4) stretch out-of-phase, C(31) and C(32) are very rigid and distort the symmetry of the mode; strong νC═C in P2 and weaker in P3; further very strong δ_{ip}C(2)H and δ_{ip}C(14)H and weaker δ_{ip}C(11)H, δ_{ip}C(9)H, δ_{ip}C(8)H, δ_{ip}C(5)H, and δ_{ip}C(15)H; no further contribution from the side chain
1565	Highly symmetric, accordion-like C═C stretching vibration at the phenanthrene ring; C(1)═C(2), C(13)═C(4), and C(7)═C(6) stretch in phase; the vibration is more disturbed in P3 due to the rigid position of C(27)F_3; medium δ_{ip}CH around the phenanthrene ring; no further contribution from the side chain
1525	Strong C═C stretching vibration in P3 of the phenanthrene ring with very strong δ_{ip}C(11)H, δ_{ip}C(9)H, and δ_{ip}C(8)H; also accordion-like C═C stretching vibration in P1 and P2 the phenanthrene ring similar to the one at 1565 cm^{-1} but with less intensity; no further contribution from the side chain
1431	Tentative assignment: strong C═C stretching vibration as well as δ_{ip}CH around the phenanthrene ring; δO(33)H, δC(15)H and δ_SC(16)H_2; no further contribution from the side chain
1383	Strong C═C stretching vibration as well as δ_{ip}CH around the phenanthrene ring; δO(33)H, δC(15)H and δ_SC(16)H_2; no further contribution from the side chain
1349	Very strong combined CC-stretching vibration at the phenanthrene ring; in-phase narrowing/breathing vibration (C(4)C(13), C(7)C(12)) of P1, P2, and P3 (combined with a deformation mode, see Fig. 7); νC(10)C(27); νC(27)F_3; very strong δ_{ip}C(9)H, δ_{ip}C(8)H, δ_{ip}C(11)H, δ_{ip}C(14)H, medium δ_{ip}C(2)H, δ_{ip}C(5)H, δ_{ip}C(15)H; small ωCH_2 contribution from the side chain
1279	This normal mode is spread across the whole molecule; strong combined CC-stretching/breathing vibration at the phenanthrene ring; very strong δ_{ip}C(11)H; very strong νC(10)C(17) and δ_SC(27)F_3 (while the F atoms are rigid); medium δ_{ip}C(2)H, δ_{ip}C(14)H, δ_{ip}C(5)H, δ_{ip}C(8)H, δ_{ip}C(9)H; medium ωCH_2, ωCH_3 across the side chain
902	This normal mode is delocalized across the whole molecule; strong asymmetric breathing vibrations at P1, P2, and P3 of the phenanthrene ring; medium δ_{ip}C(2)H, δ_{ip}C(14)H, δ_{ip}C(5)H, δ_{ip}C(8)H, δ_{ip}C(9)H; δ_{ip}C(11)H; strong ρCH_2, ρCH_3 across the side chain
757	Strong, highly symmetric breathing vibrations at P1, P2, and P3 of the phenanthrene ring; strong νC(1)Cl(31), νC(10)C(27), δ_SC(27)F_3; δ_{ip}C(15)H; ρC(16)H_2, ρC(17)H_2

The assignment was performed with help of DFT calculation [B3LYP/6–311+$G(d,p)$]. The atomic numbering scheme, as shown in Fig. 1, is used for the assignment. The atomic displacements of the prominent mode at 1622 cm^{-1}, which is strongly enhanced with UV excitation λ_{exc}=244 nm [Fig. 2(a)], is shown in Fig. 5. The atomic displacements of the strongest mode in the non-resonant Raman spectrum [Fig. 2(b)] at 1349 cm^{-1} is shown in Fig. 7.

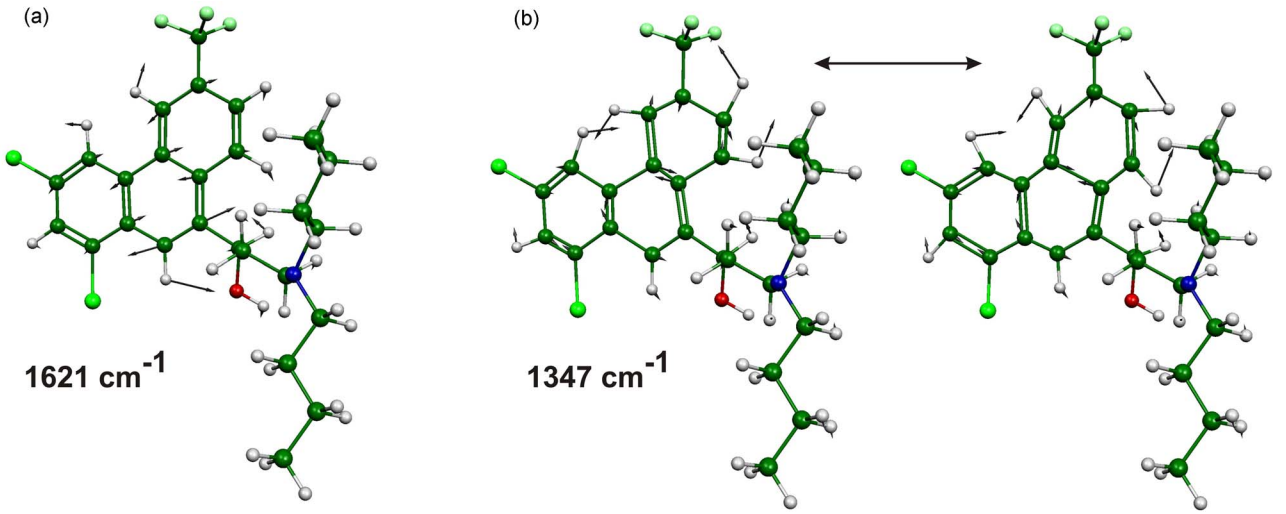

Fig. 7 (a) Calculated [B3LYP/6-311+$G(d,p)$] atomic displacements of the prominent normal mode of halofantrine at 1621 cm^{-1}. This Raman band is strongly enhanced with UV excitation $\lambda_{exc}=244$ nm [see Fig. 2(a)]. The normal mode is localized at the phenanthrene ring with very strong contributions from P1 (see Fig. 1) as described in the context. (b) Calculated [B3LYP/6-311+$G(d,p)$] atomic displacements of the prominent normal mode of halofantrine at 1349 cm^{-1}. This Raman band is very strong in the FT-Raman spectrum $\lambda_{exc}=1064$ nm [see Fig. 2(b)]. The normal mode represents a highly symmetric stretching/narrowing vibration, localized at the phenanthrene ring, as described in the text.

functional groups in the halofantrine molecule cause weak Raman signals, but very strong IR bands. All IR and Raman bands of halofantrine are shown in Fig. 6. The wave number values of some prominent IR and Raman bands are given in the Figs. 6(c) and 6(d), respectively. The strongest IR bands of halofantrine are seen at wave number values 2961, 1320, 1147, 1126, 1082, and 1049 cm^{-1}. The atomic displacement of the very strong IR mode at 2961 cm^{-1} is exemplarily shown in Fig. 8. This mode represents a combined, asymmetric CH_2/CH_3-stretching vibration in the butyl part of the side chain of halofantrine.

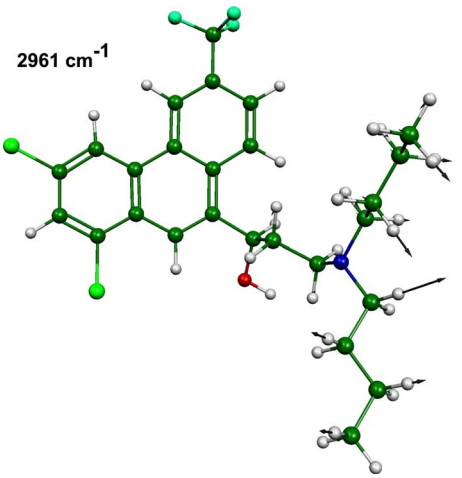

Fig. 8 Calculated [B3LYP/6-311+$G(d,p)$] atomic displacements of the prominent normal mode of halofantrine at 2961 cm^{-1}. This mode is very strong in the IR spectrum [Figs. 3(a)–3(c)] and represents a combined CH_2/CH_3-stretching vibration (polar functional group) in the side chain of halofantrine, as described in the text.

4 Conclusion and Outlook

The vibrational spectra of halofantrine, an active agent against multidrug-resistant strains of the malaria parasite *Plasmodium*, were analyzed by means of nonresonant Raman, UV resonance Raman, and IR spectroscopy as well as DFT calculations. The comparison of the nonresonant Raman spectra and UV resonance Raman spectra (Fig. 2) showed that distinct Raman bands at 1621 and 1590 cm^{-1} can be enhanced with excitation wavelength $\lambda_{exc}=244$ nm. UV resonance Raman spectra are many orders of magnitude stronger than conventional Raman spectra due to the ω^4 dependency of the scattering effect and the selective resonance enhancement. The discovery of these signal enhancements is the basis for continuing experiments that will address a localization of small concentrations of halofantrine in a biological environment. Raman microspectroscopy has unique capabilities to derive molecular information with submicrometer spatial resolution in life cells. It was possible to identify strong, combined C=C-stretching vibrations in the phenanthrene ring of halofantrine by means of a thorough mode assignment of the Raman spectra of halofantrine. These vibrations are considered as putative marker bands for $\pi\pi$ interactions with the porphyrin ring of biological target structures. The calculation of the electron density indicates a strong and even distribution across the phenanthrene ring, despite the electron withdrawing effect of the Cl and CF_3 substituents. The electron density calculation supports the hypothesis that $\pi\pi$ interactions play an important role in the molecular mode of action of halofantrine.

Further experiments are underway to monitor changes of the putative Raman marker bands during the drug-target binding process. These results will shed more light on suggested models for the biological activity of halofantrine.[20,21] A better elucidation of the molecular mode of action of halofantrine

will assist in structure-based design of new, effective antimalarials.

Acknowledgments

The authors gratefully acknowledge that computations were run at the computing center of the University Leipzig. Halofantrine was a kind gift of GlaxoSmithKline.

References

1. R. W. Snow, C. A. Guerra, A. M. Noor, H. Y. Myint, and S. I. Hay, "The global distribution of clinical episodes of *Plasmodium falciparum* malaria," *Nature* **434**(7030), 214–217 (2005).
2. WHO, "Key facts," *Rollback Malaria* website (2009), http://rbm.who.int
3. B. Witkowski, A. Berry, and F. Benoit-Vical, "Resistance to antimalarial compounds: Methods and applications," *Drug Resist Update* **12**, 42–50 (2009).
4. R. G. Ridley, "Medical need, scientific opportunity and the drive for antimalarial drugs," *Nature* **415**, 686–693 (2002).
5. I. M. Hastings, P. G. Bray, and S. A. Ward, "A requiem for chloroquine," *Science* **298**, 74–74 (2002).
6. T. E. Wellems, "*Plasmodium* chloroquine resistance and the search for a replacement antimalarial drug," *Science* **298**, 124–126 (2002).
7. T. Weinke, H. D. Notdurft, H. Kretschmer, K. Fleischer, T. Loscher, B. Braendli, K. Markwalder, T. Schlunk, R. Clemens, and H. L. Bock, "Halofantrine in the treatment of imported malaria in non-immune travellers," *Dtsch. Med. Wochenschr.* **118**, 254–259 (1993).
8. J. K. Baird, H. Basri, B. Subianto, D. J. Fryauff, P. D. McElroy, B. Leksana, T. L. Richie, S. Masbar, F. S. Wignall, and S. L. Hoffman, "Treatment of chloroquine-resistant *Plasmodium vivax* with chloroquine and primaquine or halofantrine," *J. Infect. Dis.* **171**, 1678–1682 (1995).
9. W. T. Colwell, V. Brown, P. Christie, J. Lange, C. Reece, and K. Yamamoto, "Antimalarial arylaminopropanols," *J. Med. Chem.* **15**, 771–775 (1972).
10. P. Minodier, G. Noel, M. Salles, K. Retornaz, H. Walters, J. C. Combes, and J. M. Garnier, "Mefloquine versus halofantrine in children suffering from acute uncomplicated falciparum malaria," *Arch. Pediatr.* **12**, S67–71 (2005).
11. N. Singh and S. K. Puri, "Modulation of halofantrine resistance after coadministration of halofantrine with diverse pharmacological agents in a rodent malaria model," *Life Sci.* **67**, 1345–1354 (2000).
12. Y. T. Kolade, C. P. Babalola, and G. K. E. Scriba, "Analysis of the antimalarial drug halofantrine and its major metabolite N-desbutylhalofantrine in human plasma by high performance liquid chromatography," *J. Pharm. Biomed. Anal.* **41**, 315–319 (2006) and references therein.
13. M. Foley and L. Tilley, "Quinoline antimalarials: mechanisms of action and resistance and prospects for new agents," *Pharmacol. Ther.* **79**(1), 55–87 (1998).
14. S. E. Francis, D. J. Sullivan Jr., and D. E. Goldberg, "Hemoglobin metabolism in the malaria parasite *Plasmodium falciparum*," *Annu. Rev. Microbiol.* **51**, 97–123 (1997).
15. L. M. B. Ursos and P. D. Roepe, "Chloroquine resistance in the malaria parasite *Plasmodium falciparum*," *Med. Res. Rev.* **22**(5), 465–491 (2002).
16. J. Wiesner, R. Ortmann, H. Jomaa, and M. Schlitzer, "Neue Antimalaria-Wirkstoffe" ["New antimalarial drugs"], *Angew. Chem.* **115**, 5432–5451 (2003) [in German].
17. D. J. Sullivan, Jr., H. Matile, R. G. Ridley, and D. E. Goldberg, "A common mechanism for blockade of heme polymerization by antimalarial quinolines," *J. Biol. Chem.* **273**, 31103–31107 (1998).
18. D. J. Sullivan, Jr., I. Y. Gluzman, D. G. Russell, and D. E. Goldberg, "On the molecular mechanism of chlorquine's antimalarial action," *Proc. Natl. Acad. Sci. U.S.A.* **93**, 11865–11870 (1996).
19. M. B. Reed, K. J. Sallba, S. R. Carusana, K. Kirk, and A. F. Cowman, "Pgh1 modulates sensitivity and resistance to multiple antimalarials in *Plasmodium falciparum*," *Nature* **403**, 906–909 (2000).
20. K. A. de Villiers, H. M. Marques, and T. J. Egan, "The crystal structure of halofantrine-ferriprotoporphyrin IX and the mechanism of action of arylmethanol antimalarials," *J. Inorg. Biochem.* **102**, 1660–1667 (2008).
21. K. A. de Villiers and T. J. Egan, "Recent advances in the discovery of Haem-targeting drugs for malaria and schistosomiasis," *Molecules* **14**, 2868–2887 (2009).
22. S. Pagola, P. W. Stephens, D. S. Bohle, A. D. Kosar, and S. K. Madsen, "The structure of malaria pagment β-haematin," *Nature* **404**, 307–310 (2000).
23. R. Buller, M. L. Peterson, Ö. Almarsson, and L. Leisirowitz, "Quinoline binding site on malaria pigment crystal: a rational pathway for antimalaria drug design," *Cryst. Growth Des.* **2**, 553–562 (2002).
24. B. N. Acharya and M. P. Kaushik, "Pharmacophore-based predictive model generation for potent antimalarials targeting haem detoxification pathway," *Med. Chem. Res.* **16**, 213–229 (2007).
25. A. Amponsaa-Karikari, N. Kishikawa, K. Ohyama, K. Nakashima, and N. Kuroda, "Determination if halofantrine and its main metabolite desbutylhalofantrine in rat plasma by high-performance liquid chromatography with on-line UV irradiation and peroxyoxalate chemilumuinescence detection," *Biomed. Chromatogr.* **23**, 101–106 (2009).
26. Y. T. Kolade, C. P. Babalola, A. A. Olaniyi, and G. K. E. Scriba, "Effect of kolanut on the pharmacokinetics of the antimalarial drug halofantrine," *Eur. J. Clin. Pharmacol.* **64**, 77–81 (2008).
27. D. Graham and V. Deckert, "Editorial–a light diagnosis," *Analyst* **134**, 1027–1028 (2009).
28. C. Krafft, B. Dietzek, and J. Popp, "Raman and CARS microspectroscopy of cells and tissues," *Analyst* **134**, 1046–1057 (2009).
29. C. Kendall, M. Isabelle, F. Bazant-Hegemark, J. Hutchings, L. Orr, J. Babrah, R. Baker, and N. Stone, "Vibrational spectroscopy: a clinical tool for cancer diagnostics," *Analyst* **134**, 1029–1045 (2009).
30. T. Frosch, S. Koncarevic, K. Becker, and J. Popp, "Morphology-sensitive Raman modes of the malaria pigment hemozoin," *Analyst* **134**, 1126–1132 (2009).
31. M. Diem, P. Griffiths, and J. Chalmers, Eds., *Vibrational Spectroscopy for Medical Diagnosis*, Wiley, New York (2008).
32. P. Lasch and J. Kneipp, *Biomedical Vibrational Spectroscopy*, Wiley-VCH, Hoboken, NJ (2008).
33. T. Frosch, S. Koncarevic, L. Zedler, M. Schmitt, K. Schenzel, K. Becker, and J. Popp, "*In situ* localization and structural analysis of the malaria pigment hemozoin," *J. Phys. Chem. B* **1**(37), 11047–11056 (2007).
34. L. Puskar, R. Tuckermann, T. Frosch, J. Popp, V. Ly, D. McNaughton, and B. Wood, "Raman acoustic levitation spectroscopy of red blood cell and *Plasmodium falciparum* trophozoites," *Lab Chip* **7**, 1125–1131 (2007).
35. T. Frosch, B. Küstner, S. Schlücker, A. Szeghalmi, M. Schmitt, W. Kiefer, and J. Popp, "*In vitro* polarization-resolved resonance Raman studies of the interaction of hematin with the antimalarial drug chloroquine," *J. Raman Spectrosc.* **35**, 819–821 (2004).
36. C. Krafft, P. Roesch, and J. Popp, in *Handbook of Molecular Biophysics*, H. G. Bohr, Ed., Wiley-VCH, Hoboken, NJ (2009).
37. T. Frosch, T. Meyer, M. Schmitt, and J. Popp, "Device for Raman difference spectroscopy," *Anal. Chem.* **79**, 6159–6166 (2007).
38. W. Kiefer, "Raman difference spectroscopy with the rotating cell," *Appl. Spectrosc.* **27**, 253 (1973).
39. M. J. Frisch, G. W. Trucks, H. B. Schlegel, G. E. Scuseria, M. A. Robb, J. R. Cheeseman, J. A. Montgomery, Jr., T. Vreven, K. N. Kudin, J. C. Burant, J. M. Millam, S. S. Iyengar, J. Tomasi, V. Barone, B. Mennucci, M. Cossi, G. Scalmani, N. Rega, G. A. Petersson, H. Nakatsuji, M. Hada, M. Ehara, K. Toyota, R. Fukuda, J. Hasegawa, M. Ishida, T. Nakajima, Y. Honda, O. Kitao, H. Nakai, M. Klene, X. Li, J. E. Knox, H. P. Hratchian, J. B. Cross, V. Bakken, C. Adamo, J. Jaramillo, R. Gomperts, R. E. Stratmann, O. Yazyev, A. J. Austin, R. Cammi, C. Pomelli, J. W. Ochterski, P. Y. Ayala, K. Morokuma, G. A. Voth, P. Salvador, J. J. Dannenberg, V. G. Zakrzewski, S. Dapprich, A. D. Daniels, M. C. Strain, O. Farkas, D. K. Malick, A. D. Rabuck, K. Raghavachari, J. B. Foresman, J. V. Ortiz, Q. Cui, A. G. Baboul, S. Clifford, J. Cioslowski, B. B. Stefanov, G. Liu, A. Liashenko, P. Piskorz, I. Komaromi, R. L. Martin, D. J. Fox, T. Keith, M. A. Al-Laham, C. Y. Peng, A. Nanayakkara, M. Challacombe, P. M. W. Gill, B. Johnson, W. Chen, M. W. Wong, C. Gonzalez, and J. A. Pople, *Gaussian 03, Revision D.01*, Gaussian, Inc., Wallingford, CT (2004).
40. A. D. Becke, "Density-functional thermochemistry. II. The effect of the Perdew-Wang generalized-gradient correlation correction," *J. Chem. Phys.* **97**, 9173–9177 (1992); A. D. Becke, "Density-

functional thermochemistry. III. The role of exact exchange," *J. Chem. Phys.* **98**, 5648–5652 (1993).
41. P. J. Stephens, F. J. Devlin, C. F. Chabalowski, and M. J. Frisch, "*Ab initio* calculation of vibrational absorption and circular dichroism spectra using density functional force fields," *J. Phys. Chem.* **98**, 11623 (1994).
42. C. Lee, W. Yang, and R. G. Parr, "Development of the Colle-Salvetti correlation-energy formula into a function of the electron density," *Phys. Rev. B* **37**, 785 (1998).
43. J. P. Perdew and Y. Wang, "Accurate and simple analytic representation of the electron-gas correlation energy," *Phys. Rev. B* **45**, 13244 (1992).
44. J. P. Perdew, J. A. Chevary, S. H. Vosko, K. A. Jackson, M. R. Pederson, D. J. Singh, and C. Fiolhais, "Atoms, molecules, solidas, and surfaces: Applications of the generalized gradient approximation for exchange and correlation," *Phys. Rev. B* **46**, 6671 (1992).
45. J. A. Pople, H. B. Schlegel, R. Krishnan, D. J. Defrees, J. S. Binkley, M. J. Frisch, and R. A. Whitside, "Molecular orbital studies of vibrational frequencies," *Int. J. Quantum Chem.* **15**, 269–278 (1981).
46. M. J. Frisch, J. A. Pople, and J. S. Binkley, "Self-consistent molecular orbital methods 25. Supplementary functions for Gaussian basis sets," *J. Chem. Phys.* **80**(7), 3265–3269 (1984).
47. W. J. Hehre, R. F. Stewart, and J. A. Pople, "Self-consistent molecular-orbital methods. I. Use of Gaussian expansions of slater-type atomic orbitals," *J. Chem. Phys.* **51**(6), 2657–2664 (1969).
48. A. P. Scott and L. Radom, "Harmonic vibrational frequencies: An evaluation of Hartree-Fock, Møller-Plesset, quadratic configuration interaction, density functional theory, and semiempirical scale factors," *J. Phys. Chem.* **100**, 16502–16513 (1996).
49. A. A. El-Azhary and H. U. Suter, "Comparison between optimized geometries and vibration frequencies calculated by the DFT methods," *J. Phys. Chem.* **100**, 15056–15063 (1996).
50. J. Baker, A. A. Jarzecki, and P. Pulay, "Direct scaling of primitive valence force constants: An alternative approach to scaled quantum mechanical force fields," *J. Phys. Chem. A* **102**, 1412–1424 (1998).
51. G. Rauhut and P. Pulay, "Transferable scaling factors for density functional derived vibrational force fields," *J. Phys. Chem.* **99**, 3093–3100 (1995).
52. M. D. Halls and B. Schlegel, "Comparison of the performance of local, gradient-corrected, and hybrid density functional models in predicting infrared intensities," *J. Chem. Phys.* **109**(24), 10587–10593 (1998).
53. M. P. Andersson and P. Uvdal, "New scale factors for harmonic vibrational frequencies using the B3LYP density functional method with the triple-ζ basis set 6–311+G(d,p)," *J. Phys. Chem. A* **109**, 2937–2941 (2005).
54. C. W. Bauschlicher and S. R. Langhoff, "The calculation of accurate harmonic frequencies of large molecules: the polycyclic aromatic hydrocarbons, a case study," *Spectrochim. Acta, Part A* **53**, 1225–1240 (1997).
55. T. Frosch, M. Schmitt, G. Bringmann, W. Kiefer, and J. Popp, "Structural analysis of the anti-malaria active agent chloroquine under physiological conditions," *J. Phys. Chem. B* **111**(7), 1815 (2007).
56. T. Frosch, M. Schmitt, and J. Popp, "*In situ* UV resonance Raman micro-spectroscopic localization of the antimalarial quinine in cinchona bark," *J. Phys. Chem. B* **111**(16), 4171–4177 (2007).
57. T. Frosch, M. Schmitt, and J. Popp, "Raman spectroscopic investigation of the antimalarial agent mefloquine," *Anal. Bioanal. Chem.* **387**, 1749–1757 (2007).
58. T. Frosch, M. Schmitt, T. Noll, G. Bringmann, K. Schenzel, and J. Popp, "Ultrasensitive *in situ* tracing of the alkaloid dioncophylline A in the tropical liana triphyophyllum peltatum by applying deep-UV resonance Raman microscopy," *Anal. Chem.* **79**(3), 986–993 (2007).
59. T. Frosch, M. Schmitt, K. Schenzel, J. H. Faber, G. Bringmann, W. Kiefer, and J. Popp, "*In vivo* localization and identification of the antiplasmodial alkaloid dioncophylline A in the tropical Liana triphyophyllum peltatum by a combination of fluorescence, near infrared Fourier transform Raman microscopy and density functional theory calculations," *Biopolymers* **82**(4), 295–300 (2006).
60. T. Frosch and J. Popp, "Relationship between molecular structure and Raman spectra of quinolines," *J. Mol. Struct.* **924–926**, 301–308 (2009).
61. D. A. Long, *The Raman Effect*, Wiley, New York (2002).
62. G. J. Puppels, F. F. M. De Mul, C. Otto, J. Greve, M. Robert-Nicoud, D. J. Arndt-Jovin, and T. M. Jovin, "Studying single living cells and chromoscomes by confocal Raman microspectroscopy," *Nature* **347**, 301–303 (1990).
63. T. G. Spiro, Ed., *Biological Applications of Raman Spectroscopy*, Vols. **1–3**, Wiley, New York (1988).
64. R. Petry, M. Schmitt, and J. Popp, "Raman spectroscopy: A prospective tool in the life sciences," *ChemPhysChem* **4**, 14 (2003).
65. J. M. Chalmers and P. R. Griffiths, Eds., *Handbook of Vibrational Spectroscopy. Vol. 5. Applications in Life, Pharmaceutical and Natural Sciences*, Wiley & Sons, Chichester, UK (2002).
66. T. Frosch, N. Tarcea, M. Schmitt, H. Thiele, F. Langenhorst, and J. Popp, "UV Raman imaging-a promising tool for astrobiology: comparative Raman studies with different excitation wavelengths on SNC martian meteorites," *Anal. Chem.* **79**, 1101–1108 (2007).
67. A. Taillardat-Bertschinger, C. S. Pery, A. Galland, R. J. Prankerd, and W. N. Charman, "Partitioning of halofantrine hydrochloride between water, Micellar solutions, and soybean oil: Effects on its apparent ionization constant," *J. Pharm. Sci.* **92**, 2217–2228 (2003).